VECTORIAL MULTI-PHASE MOUSE BRAIN TUMOR SEGMENTATION IN T1-T2 MRI

V. Israel-Jost[1]*, E. Breton*[2]*, E. D. Angelini*[1]*, Ph. Choquet*[2]*, I. Bloch*[1]*, A. Constantinesco*[2]

[1]Institut Telecom, Telecom ParisTech - CNRS LTCI, Paris, France
[2] HUS, Hôpital de Hautepierre, Strasbourg, France

ABSTRACT

An automated, level-set based, segmentation framework is proposed in this work for computation of tumoral volumes on mice brain bearing gliomal tumors. T1 and T2 weighted MRI images were acquired to monitor tumor growth, at different time points. We developed an original multi-phase and multi-channel segmentation method, based on the level set framework of Chan and Vese, to facilitate the estimation of tumoral volumes. A clinical study comparing manual and segmented volumes on 18 mice demonstrate the adequacy of the multi-channel segmentation and its superiority over single-T1 channel automated segmentation in terms of measurement accuracy and correlation.

Index Terms— Segmentation, level set, MRI, multi-phase, multi-channel, mice imaging, brain tumor

1. INTRODUCTION

Small animal models of human diseases constitute a major step for *in vivo* evaluation of novel therapies. Preclinical imaging provides quantitative data, allowing *in vivo* studies of therapy strategies. In this work, we use 0.1T MRI data to follow the evolution of an orthotopic brain tumor model in mice. Two 3D isotropic datasets (T1 and T2-weighted) are acquired in order to directly estimate the volume of the tumor as well as the edema involving the neighboring tissues. This volumetric approach differs from tumor size estimations with 2D parameters (such as the largest diameters), which are commonly used in tumor models. Even though diameter measurements are fast to perform and offer a first estimation of tumor volume, this method relies on a gross approximation of the tumor's shape with an ellipsoid. To avoid such assumptions on tumor shape, volumetric 3D data needs to be segmented to get a true estimation of tumor volumes. To alleviate the segmentation task, which has been manually performed so far, we propose a fully automated multi-phase and multi-channel segmentation method, based on the level set framework of Chan and Vese [1], which leads to an optimal partition of the image data in *n* homogeneous phases. In our application, one or several phases represent the tumor, thus simplifying computation of its volume, by manually selecting a region of interest around it. While several segmentation methods have been designed for brain tumor segmentation, as reviewed in [2], none were proposed based on a multiphase level set framework. An analogous work from Drapaca et al. [3], applied a multiphase level set segmentation framework to brain MRI but was limited to a single protocol.

The remaining of this paper is organized as follows: In Section 2, we describe the data acquisition setup; In Section 3, we describe the extension of the Chan and Vese [1] multi-phase level set framework to combine T1 and T2-weighted information; In Section 4, we describe and discuss results from a clinical study on 18 mice data sets comparing volumes measurements from manual thresholding, multi-phase and multi-phase/multi-channel segmentation results.

Thanks to INCA, GET grant, Région Alsace and GE Healthcare for funding.

2. DATA ACQUISITION SETUP

Animal experiments were conducted in compliance with the French guidelines for the care and use of research animals (authorization A6748220). Four adult female Swiss nude mice weighting approximately 20g were inoculated with human glioblastoma cells (5.10^5 U-87-MG cells line in 5μL PBS) into the striatum of the right hemisphere via a stereotactic injection at day 0.

Animals were weekly screened with MRI from week 1 to euthanasia (week 4 or 5). MRIs were acquired using a dedicated 0.1T resistive magnet (Bouhnik SAS, Velizy-Villacoublay, France) [4], as previously described in [5]. During imaging procedures, mice were maintained under gaseous anesthesia (isoflurane 1-1.5% in air) in a warmed-up MR-compatible technical cell dedicated to small animal imaging (Minerve, Esternay, France), which aimed at maintaining the animal homeostasis and standardized the animal positioning. After an intra-peritoneal injection of 1 mL of an MRI contrast agent, gadoteric acid (Gd-DOTA, Dotarem, Guerbet, France) at a dose of 5-6 mmol/kg body weight, T1-weighted (FAST sequence, isotropic voxel 0.5mm$\times$ 0.5mm$\times$ 0.5mm, TE 7ms; TR 100ms, 80°, cubic FOV 32mm, acquisition matrix 64$\times$ 64, 64 slices, NEX 8, acquisition time 56min) and T2-weighted (FISP sequence, reconstructed voxel 0.5mm$\times$ 0.5mm$\times$ 0.5mm, TE 14ms; TR 21ms, 70°, cubic FOV 32mm, acquisition matrix 64$\times$ 48, 32 slices, NEX 60, acquisition time 32min) images were acquired on the entire mouse brain.

A total of 18 data sets (T1 and T2-weighted) were acquired during tumor growth. As already described in [5], the presence of gadolinium contrast agent enlightens the tumor in T1-weighted images and indicates that the blood brain barrier is broken. In T2-weighted images, tumor tissue modifications and peri-tumoral edema are both visible. The two MRI protocols provide complementary information on tumoral anatomy with a redundancy on tumor tissue volume and the addition of the edema volume in T2-weighted data.

3. MULTI-PHASE AND MULTI-CHANNEL SEGMENTATION

In the present study, automated segmentation of joint T1- and T2-weighted mice brain MRI data sets is a challenging task, due to poor image resolution compared to the size of the observed structures, leading to partial volume effects and the absence of clear edges defining structures. For this reason, we chose to use the Chan and Vese [1] level set segmentation framework, based on the model of Mumford-Shah [6], which enables to segment objects according to

their average values. By doing so, we can detect zones which are not delimited by sharp edges, but rather by a variation of their average intensities. In addition, working in a multi-phase framework enables to detect several objects and, therefore, to be more sensitive to small intensity variations. For the proposed application on mice brain MRI data, using 8 phases, we were able to obtain at least one phase including only tumoral tissue in all 18 cases. We followed the implementation proposed by Chan and Vese in a level set framework, which is based on the minimization of an energy functional composed of a regularization term and a term that drives the contours toward the interface of homogeneous regions in the image. The level set framework also permits us to process n-D data with no further adaptation of the method.

In this work, we used three level set functions so as to create up to 2^3 phases, defined by the sign of the level set functions. Eight phases were required to take into account the background, the brain, the skull and scalp, one or two regions for the tumor and the edema, and other tissues.

To simplify the notations, we recall the form of the energy functional for only two level set functions Φ_1 and Φ_2, as applied in [7] for brain segmentation. We first define a phase $j \in \{00, 01, 10, 11\}$, where, for example, the index 10 corresponds to $\Phi_1 > 0$ and $\Phi_2 < 0$. Let the heterogeneity measure for each point M of the image $I : \Omega \rightarrow \mathbb{R}$, given a real value c^j associated to phase j, be defined as:

$$z^j(M) = \frac{\mid I(M) - c^j \mid^\alpha}{(\max_{P \in \Omega} I(P))^\alpha}. \tag{1}$$

We point out here that this function is commonly called a homogeneity measure in the original papers describing this segmentation framework. Since level set functions are controlled by high values of this function, we rather call it a heterogeneity measure, to be minimized in the optimization process. The positive exponent α was taken equal to 0.4, thus departing from the traditional quadratic heterogeneity measure. This results in acceleration of the convergence rate, as was shown in [8]. In this case, c^j values are no longer computed as average values on region j. Since it is difficult to provide an analytic expression of c^j for $\alpha = 0.4$, we performed an exhaustive search in the range of the pixel values in I, minimizing the derivative of z^j.

This heterogeneity measure is then used in the energy functional, with $c = (c^{00}, c^{01}, c^{10}, c^{11})$ and $\Phi = (\Phi_1, \Phi_2)$:

$$\begin{aligned} E_4(c, \Phi) = \nu \left(\sum_{i=1,2} \int_I \mid \nabla H(\Phi_i(M)) \mid \mathrm{d}M \right) \\ + \int_\Omega z^{00}(1 - H(\Phi_1))(1 - H(\Phi_2))(M)\mathrm{d}M \\ + \int_\Omega z^{01}(1 - H(\Phi_1))H(\Phi_2)(M)\mathrm{d}M \\ + \int_\Omega z^{10}H(\Phi_1)(1 - H(\Phi_2))(M)\mathrm{d}M \\ + \int_\Omega z^{11}H(\Phi_1)H(\Phi_2)(M)\mathrm{d}M \end{aligned} \tag{2}$$

where H is the Heaviside function. This functional can be minimized with respect to c and Φ by the method of Euler-Lagrange (see [1] for details). This optimization framework suffers from an important limitation, since a given point M can only move from one phase to another phase which differs from the first one by the sign of only one level set function. Therefore, a point cannot be moved directly from phase (00) to phase (11), and must transit by either (10) or (01). At the same time, during the minimization process, passing by an intermediate phase is only possible when this operation decreases the global energy, which is not the case in general (see Figure 1). A proposed solution to avoid this type of local minima, which is even more severe with eight phases, is to permute the phase labels along the iterations, which permits all the transitions between phases to happen. In the example provided in Figure 1, 250 iterations were required to perform all the necessary permutations on the phase labels. With this modification of the numerical implementation, the method performed robust segmentation of the 3D brain phantom (one manually labeled IBSR dataset with a simulated 3D tumor and edema added) with eight phases. All piece-wise constant tissues were correctly extracted. Although the phantom is noise free, extracting the eight different tissues could still be challenging when evolving exactly eight phases, given the existence of local minima in which the segmented regions could be trapped. It was therefore necessary to employ our phase relabelling, since the original implementation of Chan and Vese was only able to extract six or seven regions, because of the aforementioned problem. This is illustrated in Figure 1, where only one slice of the volume is shown, with five distinct regions. We always used the initialization recommended in [1] (i.e. cylinders equally distributed in the image) as well as the semi-implicit scheme described in the same paper, with $\Delta t = 10$ and $\nu = 1.5$.

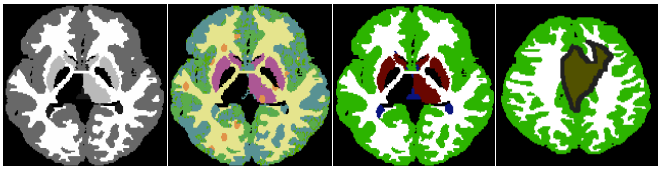

Fig. 1. From left to right: IBSR phantom; 8-phase segmentation result with the original implementation. Orange disks are residual traces of initial conditions, composed of points which could not be moved in the optimal region; 8-phase segmentation result with phase relabelling. Only five distinct regions are present in this slice; 8-phase segmentation result with phase relabelling (different slice with added tumor and edema).

Multi-channel segmentation can be performed as an extension of the multi-phase method, using a fusion rule between the heterogeneity measures z_1^j and z_2^j, associated with two images $I_1, I_2 : \Omega \rightarrow \mathbb{R}$. A multi-channel framework has already been proposed by Chan, Sandberg and Vese [9] (the so-called 'vector model') as an extension of the two-phase *Active contour without edges* of Chan and Vese. The same group of authors later improved their own method in [10], by pointing out that the segmentation obtained by using a sum of the heterogeneity measures over the different channels to fuse information, as was done in their vector model [9], generally converges to a local minimum of the energy. Their 'logic-based framework' corrected this limitation by using different fusion rules inside and outside the contour, leading to a global optimal solution and a better grasp of the logic operations performed by the model. However, none of these methods was applied in the multi-phase case, and this extension is another contribution of the present work.

In order to detect a region with a distinct intensity in at least one image, we used the following fusion rule: $\max(z_1^j, z_2^j)$ (which is called a t-conorm in the fuzzy set theory) for every phase j. By doing so, the heterogeneity measure remains high (close to 1) as long as the corresponding phase is not homogeneous in *all* channels,

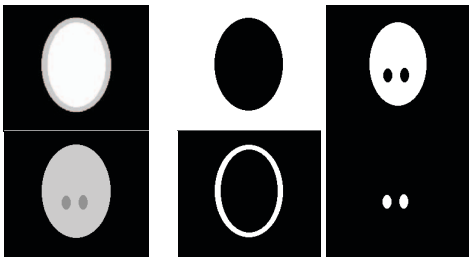

Fig. 2. Left column: multi-channel test image with two observations of the same object (up and down); right: four binary objects extracted by multi-channel segmentation.

leading to the possibility to detect all objects present in at least one image, provided that we have enough phases. In the synthetic example given in Figure 2, there are three distinct regions in each channel. The multi-channel segmentation of these two images with the above fusion rule led to the detection of four regions in the final segmentation. A linear combination of these four regions can be used to exactly generate any of the two original images. When there are more distinct regions than the number of phases, the regions associated with the closest intensity in both channels are merged into one single phase. In this general case, a linear combination of the regions computed in the segmentation process can be used to approximate any single image from the multi-channel data.

4. RESULTS AND DISCUSSION

In this clinical study, 18 mice brain datasets were acquired. The 3D isotropic MRI data was manually processed using the ImageJ software (Rasband WS, ImageJ, US NIH, Bethesda, Maryland, USA, http://rsb.info.nih.gov/ij/, 1997-2007). In both T1 and T2-weighted acquisitions, the tumor related volume of interest exhibited a hypersignal. Corresponding pixels were selected in axial slices by applying an upper threshold, which value was determined manually both by visual data analysis and by considering the data grey level histogram. Thresholding was followed by manual erasing of selected non-related areas, e.g. scalp or muscles in T1, and fat or eyes in T2-weighted data. The number of selected voxels was multiplied by the individual voxel volume (0.125mm^3) to compute the tumor related volume. Two experimented observers independently measured tumor volumes with this method in order to study inter-observer variation. One of the observers repeated the measurements three times within a month in order to determine intra-observer variations.

Results are illustrated in Figure 3 for one case, and volumes computed with manual and semi-automatic methods are visible in Figure 4 (top). We also provide a graph of the linear correlation between manual thresholding method (T1 and T2-weighted data) and our multi-phase (MP) volume estimation applied to both single channel T1 and T2-weighted data and T1 and T2-weighted multi-channel (MC) data in Figure 4 (bottom). Table 1 summarizes those results: correlation slope (Slope), intersection at the origin (y-int.) and correlation coefficient (Corr. r) were computed. Manual thresholding method reported a significant linear correlation with r=0.97 between the two independent observers. Intra-observer variation showed a mean standard deviation of 9mm^3 on tumor volumes which are clearly statistically correlated (r=0.99). This method is thus reproducible, but it is also time consuming and demands experimented observers, which may explain why tumor growth are generally described with radius measurements and ellipsoid models.

	T1 man/ T1-MP	T1 man/ MC-MP	T2 man/ T2-MP	T2 man/ MC-MP
Slope	0.56	0.97	0.75	0.83
y-int. (mm^3)	18.07	7.65	7.77	3.55
Corr. r	0.74	0.97	0.97	0.92

Table 1. Evaluation of the tumor volume estimation: linear correlation between gold standard T1 and T2 manual segmentations and T1, T2 and multi-channel (MC) semi-automatic multi-phase (MP) segmentations.

Our semi-automatic multi-phase and multi-channel segmentation method aims to reduce operator dependent tasks. Considering the average over observers of the volume measures determined with manual thresholding as the gold standard, we found for T1-weighted data a correlation coefficient r=0.74 between the gold standard evaluation and the results provided by the multi-phase segmentation (column T1/T1). For T2-weighted data, this correlation was r=0.97. Applying the original multi-phase and multi-channel segmentation increased the correlation coefficient to r=0.97 with a linear relation slope close to 1 (0.97) between the gold standard in T1 and multi-channel volumes. Considering the T2-weighted data, the correlation decreases when applying the multi-channel segmentation (r=0.92) while the slope becomes closer to 1 (0.75 to 0.83). These coefficients are in accordance with our observation that the multi-channel segmentation tends to often converge to a solution with only one phase containing the tumor, and that leaves the edema as well as the scalp in other phases.

Analysis of these results shows that using the multi-channel segmentation method, we could benefit from the information of both T1- and T2-weighted data. In particular, while the tumor and the edema can often not be separated in the T2 image, the result still provides a necessary region for the location of the tumor. In addition, this necessary region generally excludes the scalp, which has the same intensity range as the tumor in T1-weighted images, therefore considerably reducing operator dependent decisions in the multi-channel segmentation. Finally, given the limited number of phases, only the most relevant structures of each images are represented in the segmentation, which significantly simplifies the results and avoids to dedicate phases to partial volume effects.

Improvement is clearly demonstrated by a significant increase in the correlation from T1/T1-MP to T1/MC-MP, driven by the fusion rule used in the proposed framework. Yet, the multi-channel segmentation was not always able to dedicate a phase to the edema, therefore decreasing the correlation coefficient from T2/T2-MP to T2/MC-MP segmentations. Since the target quantitative data describing tumor growth is the tumor volume, while the edema is only a consequence of this disease process, the multi-channel segmentation could improve the study of tumor evolution. We believe however that the method could be further adapted to favor the presence of two phases in the vicinity of the tumor.

5. CONCLUSION

In this work, we demonstrated the feasibility of a semi-automatic computation of tumoral volumes on T1 and T2-weighted MRI of mice bearing brain tumor. Our original multi-phase and multi-

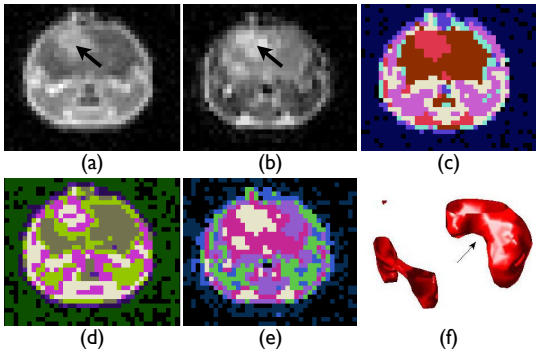

Fig. 3. Mouse MRI study, T1 (a) and T2 (b) with a tumor (arrow). Multi-channel (T1-T2) segmentation (c); multi-phase segmentation of T1 (d) and T2 (e); 3D rendering of multi-channel tumor phase, with arrow indicating the tumor (f).

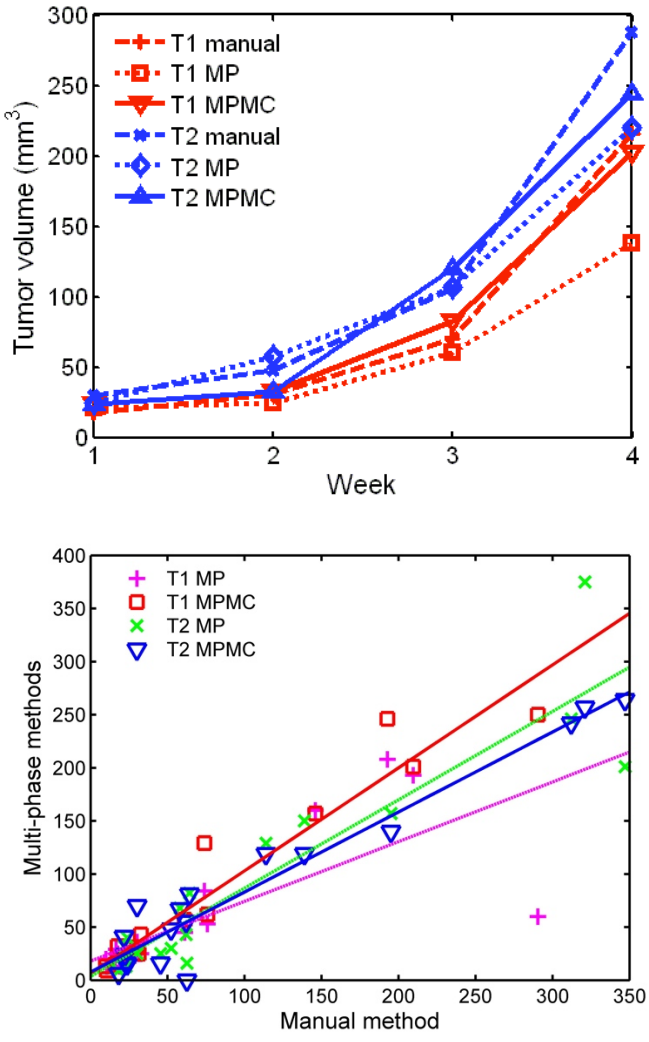

Fig. 4. Tumor volume growth over the weeks for the different segmentation methods (top) and linear correlation between semi-automatic and manual segmentation methods (bottom).

channel segmentation method extends the models proposed by Chan et al. and avoids one type of local minima affecting the original implementation.

6. REFERENCES

[1] L.A. Vese and T.F. Chan, "A Multiphase Level Set Framework for Image Segmentation Using the Mumford and Shah Model," *Int. J. Comput. Vision*, vol. 50, pp. 271–293, 2002.

[2] E. Angelini, O. Clatz, E. Mandonnet, E. Konukoglu, L. Capelle, and H. Duffau, "Glioma dynamics and computational models: A review of segmentation, registration and in silico growth algorithms and their clinical validations," *Curr. Med. Imag. Rev.*, vol. 3, pp. 262–276, 2007.

[3] C.S. Drapaca, V. Cardenas, and C. Studholme, "Segmentation of Tissue Boundary Evolution from Brain MR Image Sequences Using Multi-Phase Level Sets," *Comp. Vis. Und.*, vol. 100, pp. 312–329, 2005.

[4] S. Arbogast-Ravier, F. Xu, Ph. Choquet, B. Brunot, and A. Constantinesco, "Dedicated low field MRI: a promising low-cost technique," *Med. Biol. Eng. Computing.*, vol. 33, pp. 735–739, 1995.

[5] E. Breton, Ph. Choquet, C. Goetz, J. Kintz, J. Erbs, R. Rooke, and A. Constantinesco, "Dual SPECT/MR imaging in small animal," *Nucl. Instrum. Meth. Phys. Research A*, vol. 571, pp. 446–448, 2007.

[6] D. Mumford and J. Shah, "Optimal Approximation by Piecewise Smooth Functions and Associated Variational Problems," *Commun. Pur Appl. Math.*, vol. 42, pp. 577–685, 1989.

[7] E. Angelini, T. Song, B. D. Mensh, and A. F. Laine, "Brain MRI Segmentation with Multiphase Minimal Partitioning: A Comparative Study," *Int. J. Biomed. Imag.*, vol. 2007, pp. Article ID 10526, 15 pages, 2007.

[8] E. Angelini, T. Song, and A. Laine, "Homogeneity Measures for Multiphase Level Set Segmentation of Brain MRI," in *Proceedings of ISBI*, 2006, pp. 746–749.

[9] T.F. Chan, B.Y. Sandberg, and L.A. Vese, "Active Contours Without Edges for Vector-Valued Images," *J. Vis. Commun. Image R.*, vol. 11, pp. 130–141, 2001.

[10] B. Sandberg and T.F. Chan, "A Logic Framework for Active Contours on Multi-Channel Images," *J. Vis. Commun. Image R.*, vol. 16, pp. 333–358, 2005.